JCI The Journal of Clinical Investigation

Deficiency in Kelch protein Klhl31 causes congenital myopathy in mice

James B. Papizan, … , Ning Liu, Eric N. Olson

J Clin Invest. 2017;127(10):3730-3740. https://doi.org/10.1172/JCI93445.

Research Article **Muscle biology**

Maintenance of muscle structure and function depends on the precise organization of contractile proteins into sarcomeres and coupling of the contractile apparatus to the sarcoplasmic reticulum (SR), which serves as the reservoir for calcium required for contraction. Several members of the Kelch superfamily of proteins, which modulate protein stability as substrate-specific adaptors for ubiquitination, have been implicated in sarcomere formation. The Kelch protein Klhl31 is expressed in a muscle-specific manner under control of the transcription factor MEF2. To explore its functions in vivo, we created a mouse model of Klhl31 loss of function using the CRISPR-Cas9 system. Mice lacking Klhl31 exhibited stunted postnatal skeletal muscle growth, centronuclear myopathy, central cores, Z-disc streaming, and SR dilation. We used proteomics to identify several candidate Klhl31 substrates, including Filamin-C (FlnC). In the *Klhl31*-knockout mice, FlnC protein levels were highly upregulated with no change in transcription, and we further demonstrated that Klhl31 targets FlnC for ubiquitination and degradation. These findings highlight a role for Klhl31 in the maintenance of skeletal muscle structure and provide insight into the mechanisms underlying congenital myopathies.

Deficiency in Kelch protein Klhl31 causes congenital myopathy in mice

James B. Papizan, Glynnis A. Garry, Svetlana Brezprozvannaya, John R. McAnally, Rhonda Bassel-Duby, Ning Liu, and Eric N. Olson

Department of Molecular Biology, Hamon Center for Regenerative Science and Medicine, and Paul D. Wellstone Muscular Dystrophy Cooperative Research Center, University of Texas Southwestern Medical Center, Dallas, Texas, USA.

Maintenance of muscle structure and function depends on the precise organization of contractile proteins into sarcomeres and coupling of the contractile apparatus to the sarcoplasmic reticulum (SR), which serves as the reservoir for calcium required for contraction. Several members of the Kelch superfamily of proteins, which modulate protein stability as substrate-specific adaptors for ubiquitination, have been implicated in sarcomere formation. The Kelch protein Klhl31 is expressed in a muscle-specific manner under control of the transcription factor MEF2. To explore its functions in vivo, we created a mouse model of Klhl31 loss of function using the CRISPR-Cas9 system. Mice lacking Klhl31 exhibited stunted postnatal skeletal muscle growth, centronuclear myopathy, central cores, Z-disc streaming, and SR dilation. We used proteomics to identify several candidate Klhl31 substrates, including Filamin-C (FlnC). In the *Klhl31*-knockout mice, FlnC protein levels were highly upregulated with no change in transcription, and we further demonstrated that Klhl31 targets FlnC for ubiquitination and degradation. These findings highlight a role for Klhl31 in the maintenance of skeletal muscle structure and provide insight into the mechanisms underlying congenital myopathies.

Introduction

Skeletal muscle development and postnatal growth depend on transcriptional activation of a broad array of muscle structural genes and maintenance of protein homeostasis in an environment that is subject to intensive wear and tear. The establishment and integrity of the sarcomere, the smallest functional contractile unit of striated muscle, are vital for muscle function. Mutations in genes that encode sarcomere proteins often result in lethal or debilitating myopathies, including muscular dystrophies and nondystrophic congenital myopathies (1–3). Congenital myopathies typically manifest around birth and are characterized by structural abnormalities, including nemaline rods, centralized nuclei, and central cores (4). To date, there are no effective therapies for any of these disorders, and much remains to be learned about the underlying disease mechanisms.

Mutations in the Kelch-like proteins KBTBD13, KLHL40, and KLHL41 result in nemaline myopathy (5–8), named for the presence of nemaline bodies comprising contractile protein aggregates (9). The Kelch superfamily comprises a large, functionally diverse group of proteins that all contain an evolutionarily conserved C-terminal kelch repeat domain (10). Several Kelch-like proteins function as substrate-specific adapters for the cullin-RING ubiquitin (Ub) ligase (CRL) complex (11, 12). Specifically, Kelch-like proteins act as CRL substrate receptors by directly binding cullin3 (Cul3) through an N-terminal BTB domain and the substrate through the C-terminal Kelch repeats, targeting the substrate with ubiquitination for subsequent degradation. However, we recently demonstrated that not all Kelch-like proteins target substrates exclusively for degradation (8). Both humans and mice carrying defective mutations in *Klhl40* display nemaline myopathy (6, 8) due to the destabilization of nebulin (NEB), an essential muscle structural protein, and leiomodin3 (LMOD3), an actin nucleator, suggesting that some Kelch-like proteins may function to stabilize proteins.

While searching for myocyte enhancer factor 2–regulated (MEF2-regulated) genes in a mouse model of skeletal muscle regeneration (13), we found the skeletal muscle–specific gene *Klhl31* to be activated by MEF2. Given the importance of other Kelch-like family members in skeletal muscle biology (14) and with no previous reports of *Klhl31* in a mammalian system, we generated *Klhl31*-null mice using CRISPR-Cas9 gene editing. We show that deletion of *Klhl31* in mice results in stunted postnatal skeletal muscle growth, centronuclear myopathy, sarcomeric degeneration, Z-disc streaming, and a dilated sarcotubular network. These findings are in contrast to mutations in other muscle-specific Kelch-like family members, which result in nemaline myopathy and neonatal death (5–8). We further demonstrate that Klhl31 localizes to the sarcomere Z-disc, and by using 2 nonbiased approaches, we identified several potential Klhl31 substrates, including Filamin-C (FlnC). These findings highlight a role for Klhl31 in maintenance of muscle structure and provide necessary insight into the mechanisms underlying congenital myopathies.

Results

Skeletal muscle–specific expression of Klhl31. We discovered *Klhl31* as a gene that was significantly downregulated in differentiated myoblasts isolated from mice with satellite cell–specific deletion of *Mef2a, Mef2c,* and *Mef2d* (13). The mouse *Klhl31* promoter contains 3 MEF2 consensus-binding sites, one of which is conserved to human at approximately 500 bp upstream of the transcriptional start site (Supplemental Figure 1A; supplemental material available

Conflict of interest: The authors have declared that no conflict of interest exists.
Submitted: February 15, 2017; **Accepted:** July 19, 2017.
Reference information: *J Clin Invest.* 2017;127(10):3730–3740.
https://doi.org/10.1172/JCI93445.

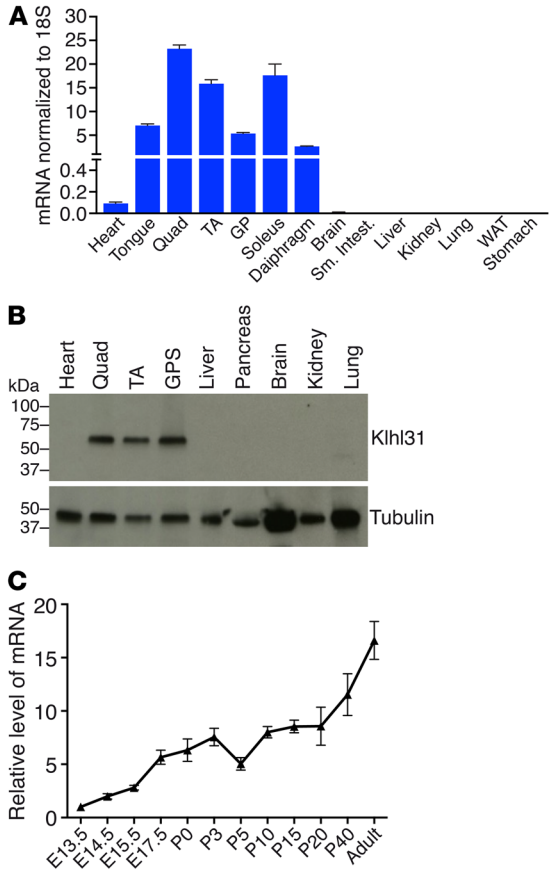

Figure 1. Skeletal muscle-specific expression of Klhl31. (**A**) Quantitative reverse-transcriptase PCR (qRT-PCR) data from a C57BL/6 multitissue library shows the *Klhl31* transcript is restricted to skeletal muscle, with relatively low levels in the heart (n = 3). Data are represented as mean ± SEM. Quad, quadriceps; TA, tibialis anterior; GP, gastrocnemius plantaris; Sm. Intest., small intestine; WAT, white adipose tissue. (**B**) Western blot analysis of Klhl31 protein expression using a C57BL/6 multitissue panel confirms that Klhl31 is expressed exclusively in skeletal muscle. GPS, gastrocnemius plantaris soleus. (**C**) *Klhl31* transcript is expressed in the embryo and increases throughout development and into adulthood in striated muscle (n = 3). Data are represented as mean ± SEM.

online with this article; https://doi.org/10.1172/JCI93445DS1). A 2-kb fragment of the mouse *Klhl31* promoter cloned into a luciferase reporter vector was activated approximately 40-fold when cotransfected with MEF2-VP16 into COS-7 cells. This induction was abrogated by about 50% when the proximal MEF2 consensus-binding site was mutated, confirming MEF2-responsive activation (Supplemental Figure 1B).

Klhl31 mRNA and protein were highly enriched in skeletal muscle tissue, with relatively low mRNA levels detected in cardiac tissue (Figure 1, A and B). Additionally, the transcript was detected in embryonic striated muscle tissue and increased in abundance after birth (Figure 1C) as well as in the C2C12 myoblast cell line following differentiation (Supplemental Figure 1C).

Loss of Klhl31 results in skeletal muscle abnormalities. To explore the role of *Klhl31* in muscle function, we generated a loss-of-function mouse model by CRISPR-Cas9 gene editing using a single guide RNA (gRNA) that targeted the first coding exon 369 bp downstream of the ATG start codon (Supplemental Figure 1D). Mosaic F_0 mice were screened for indels, and a founder with a 2-bp insertion that creates an in-frame early TAA stop codon 386 bp downstream of the ATG was chosen for further analysis. Mosaic *Klhl31* mice were backcrossed to C57BL/6 mice, and mice heterozygous for the 2-bp insertion were selected for breeding. Intercrosses of heterozygous *Klhl31*-KO mice yielded homozygous KO mice, and the loss of Klhl31 was confirmed at the mRNA and protein levels. While *Klhl31* mRNA was significantly downregulated in the KO mice (Figure 2A), immunoblotting and immunofluorescent detection methods confirmed that the protein was completely eliminated (Figure 2, B and C).

Klhl31-KO mice were born seemingly healthy, but they showed a reduction in body weight beginning around P10 (Figure 2D), and between P14 and P21, the KO mice were visibly distinguishable from their WT littermates (Figure 2E). The change in body weight coincided with a decrease in the mean cross-sectional area (CSA) of myofibers at P10, indicative of impaired postnatal muscle growth (Figure 3, A and B). To determine whether the loss of body weight was due to a decrease in muscle weight or the weight of other organs, we weighed several different muscle groups and organs in 6-week-old mice. Every muscle group tested weighed significantly less in the KO mice compared with WT, while other organ weights were unchanged (Supplemental Figure 2, A–D). Although the KO mice demonstrated hypotrophic myofibers by P10, further histological analysis revealed normal myonuclear positioning and unaltered H&E and desmin staining (Supplemental Figure 3, A and B). However, by 4 weeks of age, in addition to having hypotrophic myofibers, KO mice began to exhibit an accumulation of internalized myonuclei and pathological desmin aggregation (Supplemental Figure 3C), which was further exacerbated by 12 weeks of age (Figure 3, C and D). Additionally, protein aggregates, centralized nuclei, and a paucity of sarcomeric proteins could easily be detected in longitudinal sections by H&E staining of quadriceps (Supplemental Figure 3D). Membrane proteins involved in muscular dystrophies (15, 16), however, were unperturbed (Supplemental Figure 4).

Assessment of the mitochondrial architecture and the sarcoplasmic reticulum (SR) networks by NADH-tetrazolium reductase (NADH-TR) staining revealed an increase in the number of oxidative fibers, core-like lesions, and rubbed out fibers in the KO mice

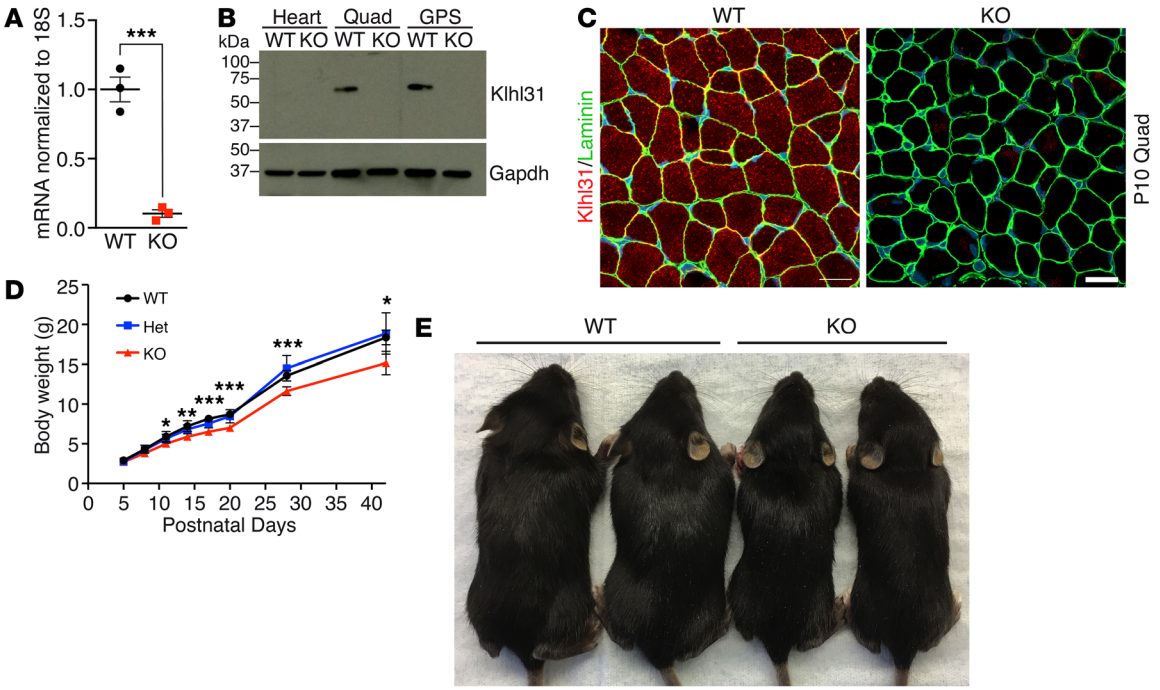

Figure 2. CRISPR-Cas9 gene editing eliminates Klhl31 protein and causes body weight reduction in *Klhl31*-KO mice. (**A**) qRT-PCR of 6-week-old WT and *Klhl31*-KO quadriceps shows a significant reduction in the *Klhl31* transcript ($n = 3$ for both genotypes). ***$P < 0.001$. (**B**) Western blot analysis showing loss of Klhl31 protein in skeletal muscle at P10. (**C**) Immunofluorescent detection of Klhl31 protein in P10 quadriceps of WT and *Klhl31*-KO mice. Scale bar: 20 μm. (**D**) Body weight curve of WT and *Klhl31*-KO mice (WT, $n = 5$; HET, $n = 17$; and KO, $n = 5$). *$P < 0.05$; **$P < 0.01$; ***$P < 0.001$, WT versus KO. Data are presented as mean ± SEM. (**E**) Representative images of 2-week-old *Klhl31*-KO mice with WT littermates. Statistical analyses were performed using an unpaired 2-tailed Student's *t* test.

by 4 weeks of age (Figure 3E). Electron microscopy also revealed an increase in the number of mitochondria in KO mice compared with WT littermate controls (Figure 3F), consistent with the increased NADH-TR staining. In addition, the KO mice contained clusters of myofibrils that lacked discernible myofilaments (Figure 3F), a feature that was even more pronounced in older animals (Figure 3G). Pleomorphic dense structures and Z-disc streaming were also present in the KO animals, and in some instances, the Z-disc was completely degenerated (Figure 3F). Older animals exhibited sarcomeric disarray, myofibril degeneration, and an immensely dilated SR network (Figure 3G and Supplemental Figure 5, A and B).

Next, we tested the biological effects of Klhl31 loss of function by subjecting 6-week-old male mice to grip-strength tests. *Klhl31*-KO mice showed a significant decrease in muscle strength in both the forelimbs and hind limbs compared with WT mice (Figure 3H). These findings indicate an essential role for Klhl31 in maintaining postnatal skeletal muscle integrity and function.

Klhl31 localizes predominantly to the Z-disc. Immunostaining of isolated myofibers showed colocalization of Klhl31 with desmin (Figure 4A) and a complete overlap with the Z-disc protein α-actinin (Figure 4B), suggesting that Klhl31 is localized to the Z-disc and cytoskeletal network. No immunostaining for Klhl31 was observed in isolated myofibers from *Klhl31*-KO mice (Supplemental Figure 6), confirming the specificity of the antibody. While we saw no nuclear localization of Klhl31 in vivo, a previous report suggested that Klhl31 localizes to the nucleus and cytoplasm when overexpressed in COS-7 cells (17). To test this and to further validate our antibody, we also transfected COS-7 cells with a myc-tagged Klhl31 expression plasmid and costained the cells using antibodies that recognize myc or Klhl31. When these cells were visualized, only the cells that were transfected with myc-Klhl31, as evidenced by myc staining, were immunoreactive to the Klhl31 antibody, highlighting the cytoplasmic localization and the specificity of the Klhl31 antibody (Figure 4C). As a control, and to be confident that our Klhl31 antibody did not detect myc, we transfected a myc-tagged Bag3 expression plasmid into COS-7 cells and similarly costained the cells with antibodies that recognize myc or Klhl31. Cells that were transfected with myc-Bag3 were positive for the myc signal, but were negative for any signal when stained with the Klhl31 antibody (Figure 4D). These findings demonstrate that the cytoplasmic Klhl31 protein predominantly localizes to the Z-disc in skeletal muscle. This localization differs from that of Klhl40, another muscle-specific kelch-like protein, which was reported to localize to the A- and I-bands (6–8).

Dysregulated sarcomeric, mitochondrial, and SR proteins in Klhl31-KO mice. Kelch-like proteins are generally thought to act as substrate-specific adaptors for Cul3-mediated protein degradation through the Ub proteasome system (UPS) (11, 12). Indeed, in coimmunoprecipitation assays in COS-7 cells, we observed a strong interaction between myc-tagged Cul3 and a 3XFlag-tagged Klhl31, suggesting that Klhl31 could be involved in a CRL complex (Figure 5A).

To identify potential substrates of Klhl31, we performed a tandem affinity purification (TAP) of 3XFlag-HA–tagged Klhl31 in C2C12 myotubes, followed by mass spectrometry (MS). In parallel, we performed proteomic analysis of 4-week-old WT and *Klhl31*-KO quadriceps to identify differentially expressed proteins in vivo (see

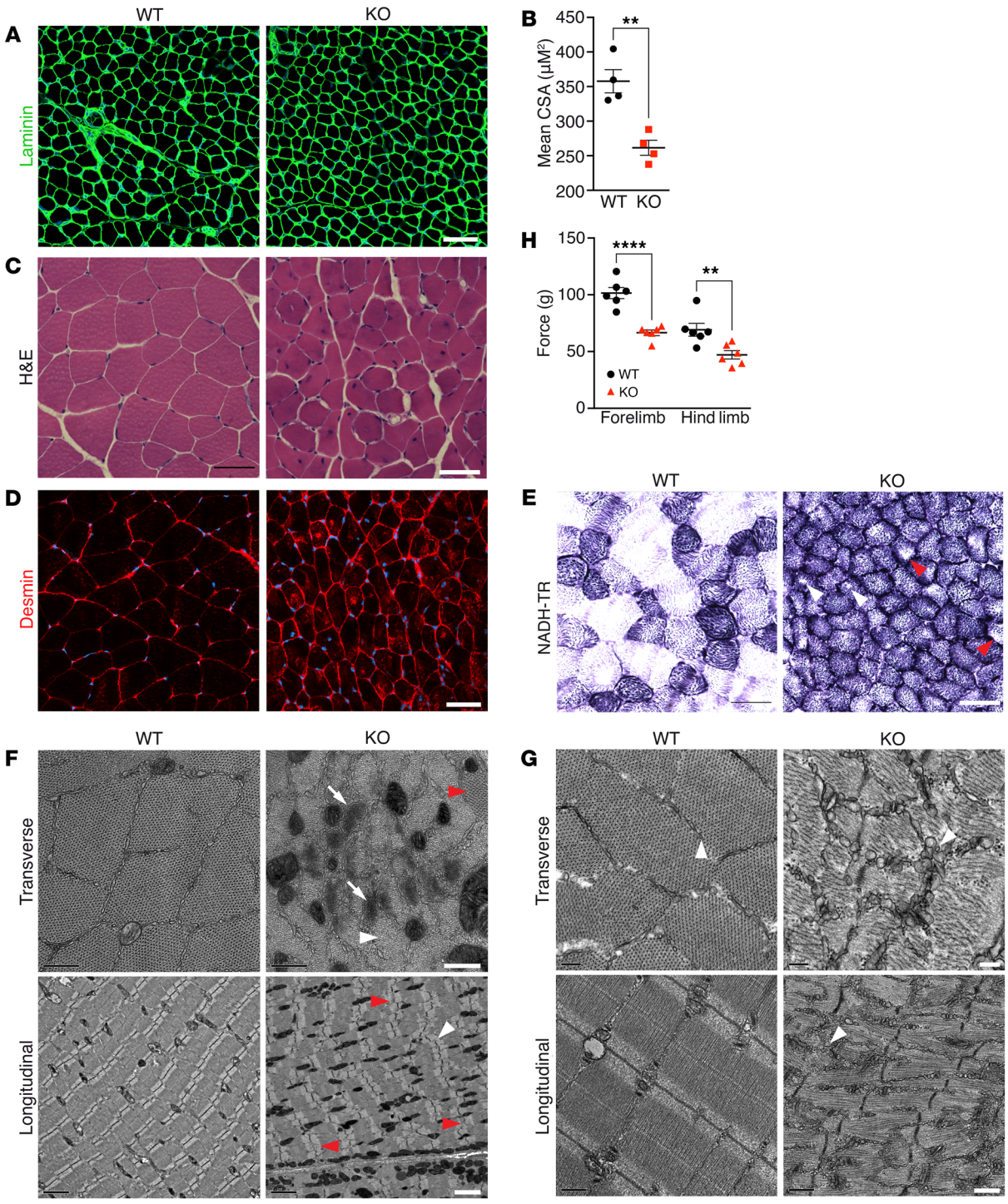

Figure 3. Loss of Klhl31 causes multiple muscle abnormalities. (**A**) Laminin immunostaining of P10 WT and *Klhl31*-KO quadriceps. Scale bar: 50 μm. (**B**) Quantification of the mean CSA of WT and KO (n = 4 for both genotypes). $^{**}P < 0.01$. Data are represented as mean ± SEM. (**C**) H&E staining of quadriceps muscle from 12-week-old WT (left) and KO (right) mice. Scale bar: 50 μm. (**D**) Desmin immunostaining of quadriceps from 12-week-old WT (left) and KO (right) mice. Scale bar: 50 μm. (**E**) NADH-TR staining of quadriceps from 4-week-old animals reveals a disorganized intermyofibrillary matrix, central cores (white arrowheads), and rubbed out fibers (red arrowheads) in KO. Scale bar: 50 μm. (**F** and **G**) Transmission electron microscopic images of (**F**) 4-week-old animals. In transverse orientation (top panel), KO mice show myofilament loss (white arrowhead) and pleomorphic dense structures (arrows). Red arrowhead denotes a myofibril with a normal pattern of myofilaments. In longitudinal sections (lower panel), numerous mitochondria are evident, Z-line streaming (white arrowhead) is abundant, and numerous Z-discs are degenerated (red arrowheads). Scale bars: 0.5 μm (upper panel); 2 μm (lower panel). (**G**) Transverse sectioning through quadriceps of 7-month-old KO animals (top panel) reveals a severely dilated SR (white arrowheads). A profound loss of myofilaments is evident in KO mice. Longitudinal sectioning demonstrates a loss of the sarcomere architecture and Z-disc continuity (white arrowhead in bottom panel). Scale bars: 0.2 μm (upper panel); 0.5 μm (low panel) (n = 3 for both genotypes). (**H**) Grip-force strength test of 6-week-old WT and KO mice. Each symbol represents the average grip force from 6 grip-force trials from an individual mouse. (n = 6 for both genotypes). $^{**}P < 0.01$, $^{****}P < 0.0001$. Data are presented as mean ± SEM. Statistical analyses were performed using an unpaired 2-tailed Student's t test.

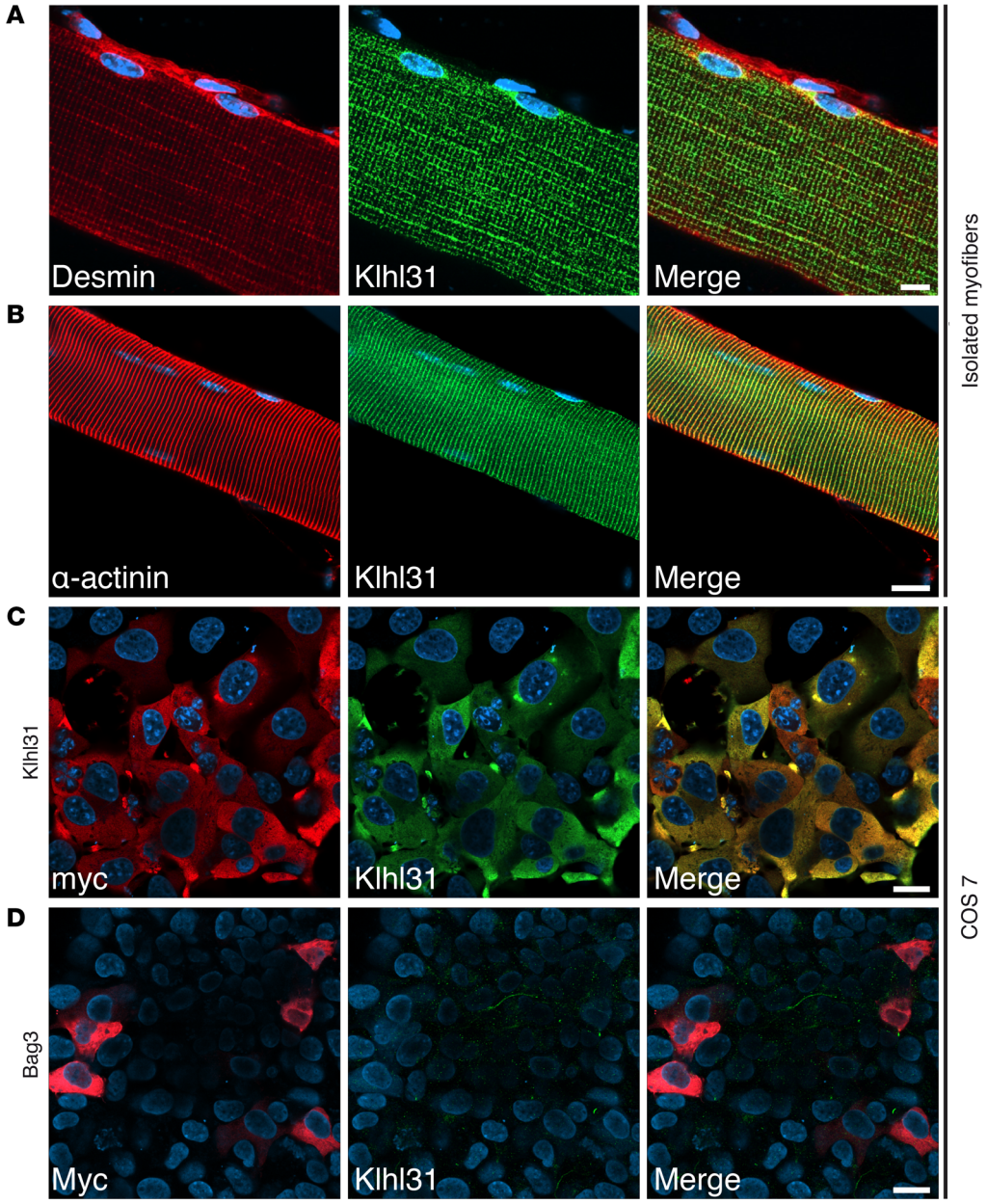

Figure 4. Klhl31 is a Z-disc protein. (**A** and **B**) Immunohistochemistry of isolated WT quadriceps myofibers stained with (**A**) desmin and Klhl31 antibodies. Scale bar: 10 μm. (**B**) α-Actinin and Klhl31 antibodies. Scale bar: 20 μm. (**C**). COS-7 cells transfected with a C-terminal Myc-tagged Klhl31 or (**D**) a C-terminal Myc-tagged Bag3 and stained with antibodies recognizing Myc and Klhl31. Scale bars: 20 μm.

Supplemental Methods). All but one of the differentially expressed proteins identified in the KO mice by proteomics were upregulated (Supplemental Table 1), suggesting that the main function of Klhl31 might be to target proteins for degradation. Six proteins in common were identified in the in vivo proteomics analysis and the TAP, including sarcomeric, SR, and mitochondrial proteins (Table 1). The differential expression of most of these proteins was confirmed by Western blot analysis and immunofluorescence (Figure 5B and Supplemental Figure 7). Moreover, the transcript levels of the identified proteins were unchanged or decreased, suggesting that the increase in protein levels was regulated posttranscriptionally (Figure 5C).

Sarcolemmal membrane-associated protein (Slmap) was the most upregulated protein identified by proteomics from the *Klhl31*-KO quadriceps (Supplemental Table 1), but was not identified by TAP in C2C12 myotubes. Slmap is a muscle-enriched, integral membrane protein and a component of the striatin-interacting phosphatase and kinase (STRIPAK) complex, which has been described as possessing roles in multiple cellular processes, including signaling, trafficking, cell migration, and cardiac function (18). Previous reports have shown that Slmap is involved in microtubule organization (19), myoblast fusion (20), and excitation-contraction coupling (21). It has also been reported that mutations in *SLMAP* may give rise to Brugada syndrome (22). Intriguingly, transgenic mice overexpressing Slmap specifically in cardiomyocytes display cardiac dysfunction and a dilated SR (23), similar to the abnormalities observed in the skeletal muscle of *Klhl31*-KO mice.

FlnC, upregulated during skeletal muscle growth 5 (Usmg5), and cytoskeletal associated protein 4 (Ckap4) were all found to be increased in abundance in *Klhl31*-KO muscle and identified by TAP. FlnC is a well-characterized Z-disc protein that repeatedly folds and unfolds during contraction, a process that makes FlnC prone to damage and require regular turnover (24). Usmg5, also

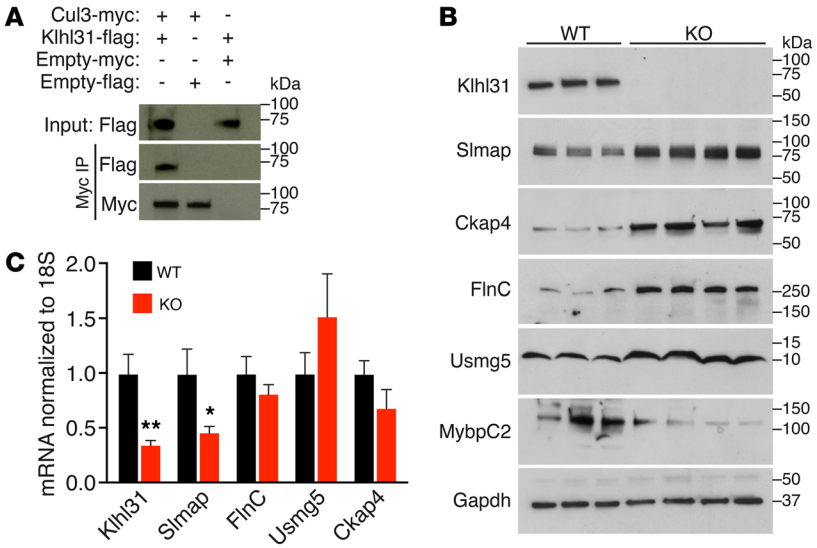

Figure 5. Dysregulated proteins in *Klhl31*-KO mice. (**A**) Coimmunoprecipitation assays show Cul3 and Klhl31 interact in transfected COS-7 cells. (**B**) Representative Western blots of 2-week-old WT and *Klhl31*-KO quadriceps (WT, $n = 3$; KO, $n = 4$). (**C**) qRT-PCR analysis of 2-week-old WT and *Klhl31*-KO quadriceps (WT, $n = 3$; KO, $n = 4$). $^*P < 0.05$; $^{**}P < 0.01$. Statistical analyses were performed using an unpaired 2-tailed Student's *t* test.

known as diabetes-associated protein in insulin-sensitive tissues (DAPIT), is a small, muscle-enriched 58–amino acid peptide that is part of the mitochondrial ATP synthase (25–27). In cell lines, Usmg5 overexpression causes mitochondrial dysfunction and glucose mishandling (28) and its overexpresssion is also seen in porcine models of Duchenne muscular dystrophy (29). Ckap4, also known as Climp-63, is a ubiquitously expressed protein and many functions have been attributed to it (30). Interestingly, the overexpression of Ckap4 has been consistently shown to cause dilation and rearrangement of the endoplasmic reticulum (31, 32), similar to the expanded and dilated SR in *Klhl31*-KO mice.

Klhl31 acts as a CRL substrate adapter. Since Klhl31 interacts with Cul3 and nearly all of the differentially expressed proteins in the KO mice were upregulated, it seems likely that Klhl31 functions primarily as a CRL substrate adapter by targeting proteins for degradation. To determine whether Klhl31 could interact with any of the proteins identified by TAP and proteomics, we performed coimmunoprecipitation experiments in transfected 293T cells. We were able to detect an interaction between Klhl31 and FlnC (Figure 6A); however, we were unable to demonstrate interaction between Klhl31 and Usmg5 or Slmap (Supplemental Figure 8). Next, we tested whether Klhl31 could ubiquitinate FlnC. In transfected 293T cells, FlnC expression was nearly ablated in the presence of Klhl31, Cul3, and WT Ub (Figure 6B). Conversely, the addition of a mutant K48R Ub or the absence of Klhl31 had no effect on FlnC expression (Figure 6B). FlnC polyubiquitination could be observed in the presence of Klhl31 and WT Ub by immunoprecipitating FlnC and immunoblotting against Ub. Consistent with these findings, in the presence of the mutant K48R Ub, we observed an intense band at the appropriate size of FlnC with diminished polyubiquitination, suggesting FlnC is ubiquitinated but cannot polymerize the K48-linked Ub chain required for proteasomal degradation (Figure 6B). In addition, we were able to detect large FlnC aggregates in *Klhl31*-KO skeletal muscle (Figure 6C), which is also observed in both humans and mouse models of FlnC myopathies (33, 34). Given that Klhl31 interacts with FlnC and not Slmap or Usmg5, it is likely that the primary defect in *Klhl31*-KO mice is Z-disc instability due to accumulation of FlnC and that the upregulation of Slmap and Usmg5 is secondary. Furthermore, transgenic mice expressing *Slmap* (Slmap-TG) under the control of the skeletal muscle actin (SKA) promoter did not exhibit centronuclear myopathy or central core disease; however, Slmap-TG mice had significantly smaller myofibers (Supplemental Figure 9, A–D). We therefore looked at the expression of FlnC Slmap and Usmg-5 proteins in younger animals and confirmed that FlnC upregulation precedes the increased levels of Slmap and Usmg5 in *Klhl31*-KO mice (Figure 6D).

Discussion

Skeletal muscle function requires the precise coordination of numerous proteins organized into the highly structured sarcomere. Consequently, mutations in a large number of sarcomeric proteins result in debilitating or lethal myopathies. Here, we identified the skeletal muscle–specific Kelch-like protein Klhl31 as a Z-disc protein and governor of postnatal skeletal muscle integrity. Disruption of *Klhl31* in mice resulted in congenital myopathy with a heterogeneous collection of myopathic abnormalities, including stunted postnatal skeletal muscle growth, centronuclear myopathy, central cores, myofibrillar degeneration, and a dilated sarcotubular network. By proteomics and tandem affinity capture, we identified FlnC as a substrate for Klhl31-mediated degradation and further demonstrated that Klhl31 interacts with FlnC and Cul3. Moreover, Klhl31, Cul3, and Ub were sufficient to degrade FlnC, whereas replacement of Ub with a K48R mutant Ub, or the absence of Klhl31, did not affect FlnC protein levels. Collectively, these data suggest that Klhl31 promotes the UPS-mediated degradation of FlnC. Klhl31 has previously been reported to be involved in myogenesis via Wnt/β-catenin signaling in zebrafish (35). While we undertook 2 different, unbiased approaches to uncovering Klhl31-binding partners, we found no evidence for alterations of the Wnt pathway in the *Klhl31*-KO mice.

FlnC crosslinks actin at the Z-disc and interacts with multiple other proteins (36–40). The upregulation of FlnC has been observed in myofibrillar myopathy patients harboring disease-causing mutations in FlnC that cause misfolding and aggregation of the protein as well as the aggregation of several other proteins including Bag3 and heat-shock proteins (41), which were also iden-

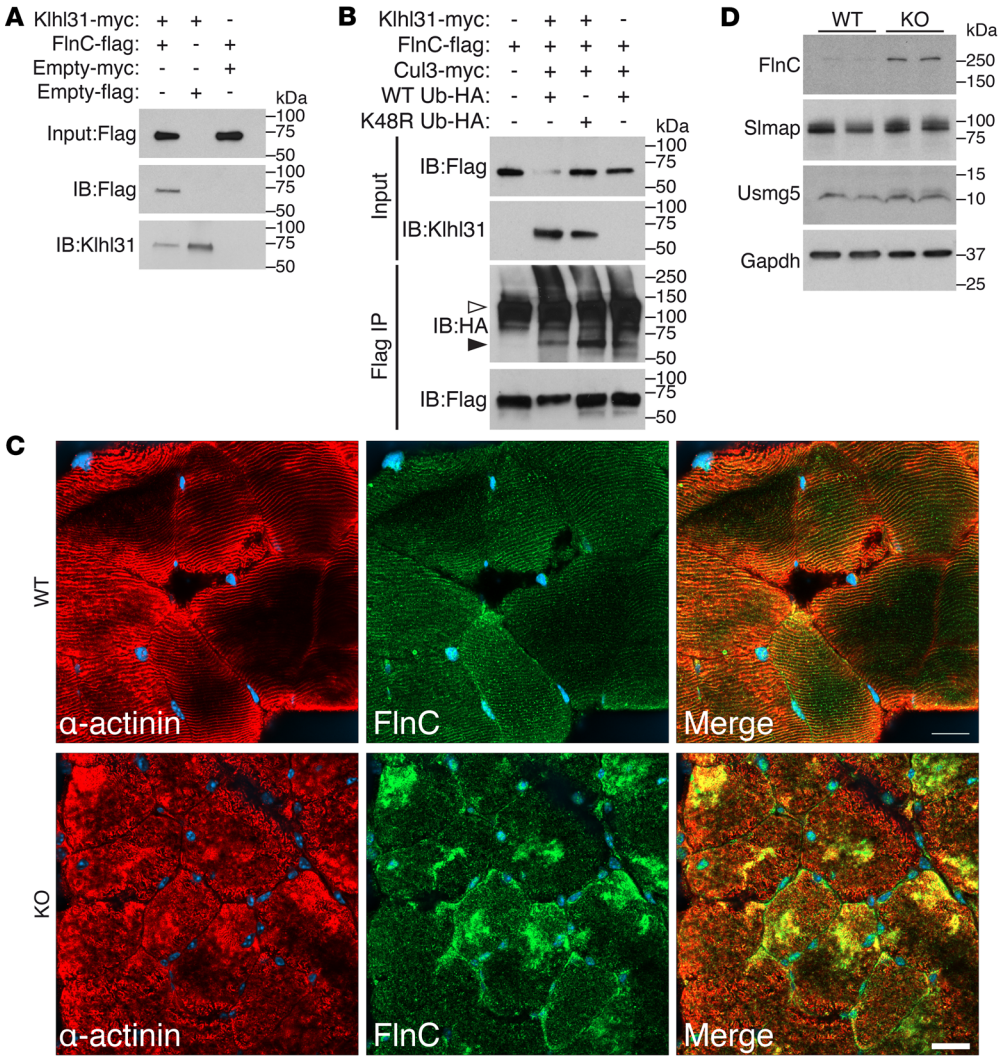

Figure 6. Klhl31 targets FlnC for ubiquitination. (**A**) Coimmunoprecipitation assay showing Klhl31 interacts with FlnC. (**B**) Transfected COS-7 cells were immunoprecipitated with anti-Flag antibody, followed by Western blotting with anti-HA antibodies. Polyubiquitination of FlnC is reduced in the presence of a K48R mutant Ub or in the absence of Klhl31. FlnC protein levels were reduced by overexpression of Klhl31, Cul3, and Ub. This reduction is rescued by the addition of the K48R mutant Ub or in the absence of Klhl31. Black arrowhead indicates increased ubiquitinated FlnC with a reduction in polyubiquitination in the presence of the K48R mutant Ub. White arrowhead indicates a nonspecific band. (**C**) Immunohistochemistry of WT and *Klhl31*-KO quadriceps with α-actinin and FlnC antibodies shows FlnC aggregates in *Klhl31*-KO mice. Scale bar: 20 μm. (**D**) Western blot analysis of WT and *Klhl31*-KO quadriceps at P10 using FlnC, Slmap, and Usmg5 antibodies.

tified by Klhl31 proteomics analyses. Chaperone-assisted selective autophagy (CASA) has been shown to control the removal of damaged Z-disc–associated proteins, including FlnC in skeletal muscle (24), while the cardiac-specific E3-ligase component F-box and leucine-rich repeat protein 22 (Fbxl22) has been demonstrated to control the Cullin-1–mediated turnover of FlnC in the heart (42). Given the abundant number of proteins associated with the Z-disc and the emerging role of this nexus as a signaling hub (43), it is not surprising that Z-disc–associated proteins would have different levels of proteostasis regulation.

Many of the upregulated proteins identified by proteomics in the *Klhl31*-KO mice are known to carry mutations that give rise to muscular dystrophies or congenital myopathies in humans, such as FlnC, αβ-crystallin, Bag3 (44), Dnajb6 (45), Lamin A/C (46), Dag1 (47), Sgcb (48), and Klhl41 (7). We cannot rule out that Klhl31 interacts with and facilitates the degradation of some of these proteins, which could account for some of the abnormalities seen in the *Klhl31*-KO mice, such as centronuclear myopathy. Many of these proteins also associate with the Z-disc, and further biochemical experiments are needed to determine whether Klhl31 promotes their degradation.

It is interesting that only 1 protein was identified as being downregulated in *Klhl31*-KO mice. A profound decrease in MybpC2 was detected and could either be attributed to (a) Klhl31 stabilizing MybpC2 in a manner similar to the effect of Klhl40 on LMOD3 and NEB (8), or, more likely, (b) the fact that following Z-disc instability in the KO mice, the sarcomere is compromised, leading to a secondary loss of thick filament proteins.

We examined the expression of proteins involved in centronuclear myopathies, including myotubularin, dynamin 2, and

Table 1. Proteins identified by proteomics of 4-week-old *Klhl31*-KO quadriceps and by TAP of C2C12 myotubes.

Protein	Proteomics: unique peptides	TAP: peptide spectrum matches
Slmap	6	N/A
Ckap4/Climp-63[A]	10	7
Filamin C[A]	70	22
Kif5b/Kinesin 1[A]	13	4
Klhl41[A]	27	18
Usmg5[A]	2	6
Grp78/HspA5[A]	24	24
MybpC2	76	N/A

[A]Proteins identified by both TAP (performed in C2C12 myotubes) and LC/LC-MS/MS proteomics.

amphiphysin 2, but were unable to detect any changes in protein levels in the *Klhl31*-KO mice. However, proteomics did detect significant changes in nuclear membrane proteins, microtubule-associated proteins, and Kif5b (Supplemental Table 1), all of which have been implicated in myonuclear positioning (49–51). Future studies will determine whether Klhl31 plays a direct role in the microtubule dynamics required for normal positioning of myonuclei.

Mutations in Trim32, another sarcomeric E3 Ub ligase, also give rise to myofibrillar degeneration and SR dilation (52, 53), although both humans and mice with Trim32 loss of function have a much more profound sarcotubular myopathy, distinguished by large intermyofibrillar vacuoles. Like Klhl31, Trim32 has also been shown to localize to and target Z-disc proteins (52, 54), and we have identified potential downstream regulators that may cause the dilated SR observed in the *Klhl31*-KO mice. Both Ckap4 and Slmap were upregulated in the KO mice, which have both been shown to cause dilation and rearrangements of the ER (21, 31, 32).

In summary, we describe the functional characterization of a new protein involved in congenital myopathy. Klhl31 is a Z-disc protein that recruits FlnC for UPS-dependent degradation. The loss of Klhl31 in mice results in nondystrophic congenital myopathy with hypotrophic fibers, Z-disc streaming, central cores, centronuclear myopathy, and late-onset sarcotubular myopathy. We propose that Klhl31 is required to maintain normal protein turnover at the Z-disc and that, in the absence of Klhl31, a toxic accumulation of proteins manifests, resulting in destabilization of the Z-disc and subsequently the myofibril. It remains to be determined whether humans with nondystrophic congenital myopathies, myofibrillar myopathies, or sarcotubular myopathies carry mutations in *Klhl31*. However, many myofibrillar myopathy cases have an unknown genetic cause (55, 56). Future studies will elucidate additional Klhl31 substrates and the upstream mechanisms that determine how and when Klhl31 interacts with its substrates and will provide much needed mechanistic insight into the pathogenesis of nondystrophic myopathies.

Methods

Generation of Klhl31-KO mice. KO mice were generated using the CRISPR-Cas9 gene-editing system by pronuclear and cytoplasmic injection of mouse embryos with *Klhl31* gRNA and Cas9 mRNA as previously described (57). In short, a gRNA targeting the first exon of *Klhl31* was cloned into PX330 (a gift from Feng Zhang, Massachusetts Institute of Technology, Boston, MA, USA; Addgene plasmid 42230) (58) and cleavage efficiency was tested in 10T1/2 mouse fibroblast cells. The gRNA was transcribed in vitro and spin-column purified, while the Cas9 mRNA was obtained commercially (TriLink Biotechnologies). Mouse embryos were injected with an equal ratio of gRNA and Cas9 mRNA into the pronucleus and cytoplasm and transferred to a surrogate dam for gestation. Mutants in the F1 generation were identified by T7E1 assay, and the alleles were cloned and sequenced. A mouse with a 2-bp insertion was chosen for further study and was backcrossed at least 4 generations on a C57BL/6 background. While both male and female mice exhibited similar myopathies, data from only male mice were reported. Mice were genotyped using a custom TaqMan genotyping assay (Life Technologies). Tail DNA was isolated on a heat block for 30 minutes using 100 μl of an alkaline lysis buffer (25 mM NaOH, 0.2 mM EDTA), followed by 100 μl of neutralization buffer (40 mM Tris-HCl). Particulates were removed by high-speed centrifugation, and the supernatant was diluted 1:10 in nuclease-free water. The DNA was then analyzed by qPCR with a mixture of the following oligonucleotides: F, CTTTAGGGCTAGCCACAGTGATC; R, AGCAGAAATGATGCTTCCTATTGTGT; WT probe, TTTCCCGTTAAGCAT-FAM; KO probe, TTCCCGTGATTAAGCAT-VIC.

Generation of SKA-Slmap transgenic mice. A SKA-Slmap transgene was generated by inserting the full-length *Slmap* ORF downstream of the SKA promoter (59). The construct contains a downstream human growth hormone ploy(A) signal. Transgenic mice were generated as previously described (60). Mice were genotyped using primers specific to the SKA promoter and the coding region of *Slmap* (Supplemental Table 2).

Grip-strength testing. Six-week-old mice were lifted by the tail, causing each mouse to grasp the pull-bar assembly connected to the grip-strength meter (Columbus Instruments). The mouse was drawn along a straight line leading away from the sensor until the grasp was broken, at which time the peak force in grams was recorded. Each trial was repeated 4 times, and all measurements were performed in a blinded fashion.

Cell culture, transfection, and luciferase reporter assays. COS-7 cells (CRL-1651, ATCC) and 293T cells (CRL-3216, ATCC) were grown and maintained in DMEM containing 10% FBS. FuGENE 6 Transfection Reagent (Promega) was used for all transfections according to the manufacturer's protocol. For luciferase assays, cells were plated onto 6-well dishes and transfected with appropriate plasmids for 48 hours. Total plasmid DNA content was kept constant by adding an empty pcDNA3.1 plasmid when necessary. For all conditions, 330 ng of each plasmid DNA was used, and 100 ng of a CMV promoter-driven *LacZ* expression plasmid was included in all transfections as an internal control. All experiments were performed in triplicate and were repeated twice.

Promoter cloning and site-directed mutagenesis. A 2-kb fragment of the *Klhl31* promoter was cloned from mouse tail genomic DNA into a pGL3b luciferase reporter (Promega). PCR-based site-directed mutagenesis of the promoter was performed using a QuikChange Lightning Site-Directed Mutagenesis Kit according to the manufacturer's guidelines (Agilent Technologies). Mutations were confirmed by DNA sequencing.

Western blot analysis. Lysates were prepared by pulverizing flash-frozen tissue. Tissue powder was homogenized in RIPA buffer (Sigma-Aldrich) with the addition of protease inhibitors (cOmplete ULTRA Mini

Tablet) on ice in a glass dounce homogenizer. Protein concentrations were determined using a BCA protein assay kit (Pierce). Samples were separated on Any kD tris-glycine buffered polyacrylamide gels (Bio-Rad) and transferred onto Immobilon P membranes (Millipore). Membranes were blocked for 1 hour at room temperature with 5% nonfat dry milk in TBST, and primary antibody hybridization was carried out overnight at 4˚C using the following antibodies: Klhl31, 1:100 (sc-132316, Santa Cruz Biotechnology Inc.); Ckap4, 1:1000 (A302-257A-T, Bethyl); Slmap, 1:1000 (A304-505A-T, Bethyl); Usmg5, 1:2000 (17716-1-AP, Proteintech); MybpC2, 1:1000 (SAB2108180, Sigma-Aldrich); FlnC, 1:1000 (ab180941, Abcam); Gapdh, 1:10,000 (MAB374, Millipore); Myc 1:1000 (51-1485GR, BD Biosciences); Flag, 1:1000 (F3165, Sigma-Aldrich); Flag-HRP, 1:2000 (A8592, Sigma-Aldrich), and Tubulin, 1:5000 (T6199, Sigma-Aldrich). Following overnight incubation in primary antibodies, the membranes were thoroughly washed in TBST and then incubated in HRP-conjugated secondary antibodies (Bio-Rad) at 1:20,000 for 1 hour of shaking at room temperature. Membranes were then developed with Western blotting luminol reagent (Sant Cruz Biotechnology Inc.) or Lumi-Light PLUS (Roche) for Klhl31 and exposed to autoradiograph film.

Histology, immunofluorescence, and electron microscopy. Following excision, skeletal muscle tissues were embedded in a mixture of OCT (Fisher) and gum tragacanth (Sigma-Aldrich) and flash-frozen in a 2-methybutane reservoir submerged in liquid nitrogen, followed by cryostat sectioning at 10 μM. Sections designated for H&E staining were fixed for 5 minutes in 10% buffered formalin at room temperature, followed by routine staining. For immunofluorescent staining, sections were air-dried for 15 minutes and fixed with 1% PFA for 2 minutes. Sections were then permeabilized for 15 minutes with PBST (0.3% Tween-20), followed by blocking with 5% donkey serum (Sigma-Aldrich) in PBST for 30 minutes. Primary antibodies were diluted in 2% donkey serum in PBST and added overnight at 4˚C in a humidified chamber using the following antibodies: Klhl31, 1:100 (sc-132316, Santa Cruz Biotechnology Inc.); laminin, 1:500 (L9393, Sigma-Aldrich); MybpC2, 1:1000 (SAB2108180, Sigma-Aldrich); Desmin, 1:1000 (clone D33, M0760, Dako); Myc 1:1000 (51-1485GR, BD Biosciences); and FlnC, 1:500 (HPA006135, Sigma-Aldrich). Images of H&E-stained slides were taken with a Keyence BZ-X700 scope, and confocal images were taken with a Zeiss LSM-800 using a 40× oil objective. Images for electron microscopy were obtained from 4-week-old and 7-month-old mice, and sections were generated as previously described (61).

Plasmid constructs and TAP. All plasmid constructs were cloned into either pcDNA3.1 C-terminal 3XFlag or His/Myc tag using quadriceps and gastrocnemius cDNA as cloning templates and Phusion High-Fidelity DNA Polymerase (NEB). The HA-tagged Ub plasmid was a gift from Ted Watson (Addgene plasmid 17608) (62). PCR-based site-directed mutagenesis of lysine-48 to an arginine was performed using a QuikChange Lightning Site-Directed Mutagenesis Kit according to the manufacturer's guidelines (Agilent Technologies). All primers are listed in Supplemental Table 2. The TAP assay was performed as previously described (8). The N-terminal Flag-tagged FlnC fragment construct has been described previously (38).

MS. MS following TAP was performed by the University of Texas Southwestern Proteomics Core Facility. The in vivo TMT labeling and 10-fraction double tandem liquid chromatography MS (LC/LC-MS/MS) was performed by the Duke University School of Medicine, Proteomics and Metabolomics Shared Resource (Durham, North Carolina, USA). Further details are described in Supplemental Methods.

Coimmunoprecipitation. Following a 48-hour transfection with FuGENE-6, cells were washed 2× with ice-cold PBS. Then 1 ml of IP buffer (20 mM $NaPO_4$, 150 mM NaCl, 2 mM $MgCl_2$, 0.1% NP40, 10% glycerol, 10 mM sodium fluoride, 0.1 sodium orthovanadate, 10 mM sodium pyrophosphate, 1 mM DTT, 1 cOmplete ULTRA Mini Tablet protease inhibitor [Roche], and 1 PhosSTOP phosphatase inhibitor [Roche]) was added to the 10-cm plate and cells were scraped and collected in an Eppendorf tube on ice. Cells were vortexed at high speed for 15 seconds to facilitate the lysis. Lysates were incubated on ice for 20 minutes, then centrifuged at 23K *g* for 20 minutes. 700 μl of the supernatant was removed and transferred to a new ice-cold Eppendorf tube. The lysate was diluted by adding an additional 700 μl of ice-cold IP buffer. 1 ml of the diluted lysate was transferred to a new Eppendorf tube, and 50 μl of washed EZview Red anti-myc or anti-flag beads (Sigma-Aldrich) was added to the lysate and rotated overnight at 4˚C. The following day, the beads were centrifuged at 8K *g* for 2 minutes, supernatant was removed, and beads were washed 2× with IP buffer. Following the last wash, IP buffer was removed, 40 μl of 2× Laemmli sample buffer (Bio-Rad) was added, and beads were boiled for 3 minutes. Beads were centrifuged at 8K *g*, and the supernatant was used for Western blot analysis (see *Western blot analysis*).

Statistics. Values are given as SEM or SD. Differences between 2 groups were assessed using unpaired 2-tailed Student's *t* tests. $P < 0.05$ was regarded as significant. Statistical analysis was performed in Prism 7 (GraphPad).

Study approval. All animal procedures were approved by the Institutional Animal Care and Use Committee at University of Texas Southwestern Medical Center.

Author contributions

JBP performed the majority of the experiments, analyzed the data, and wrote the paper. GAG performed an initial characterization of the mouse model, SB assisted in experimental studies, JRM generated the knockout and transgenic mouse lines, and RBD, NL, and ENO directed the study and helped write the paper.

Acknowledgments

We thank Robyn Leidel for assistance and advice of the University of Texas Southwestern Electron Microscopy Core Facility, Andrew Lemoff for advice with the MS analysis, and James Richardson and Dennis Burns for help with histology and imaging. We are grateful to M. Arthur Moseley, Erik Soderblom, and the Duke University School of Medicine for the use of the Proteomics and Metabolomics Shared Resource. We would also like to thank Laura Ingle and Eric Plautz of the University of Texas Southwestern Neuro-Models Facility for grip-strength testing. We are very grateful to Jose Cabrerra for assistance with graphics. This work was supported in part by grants from the NIH (DK-099653, AR-067294, HL-130253 and HD-087351) and the Robert A. Welch Foundation (grant 1-0025 to ENO). NL was supported by a Beginning-Grant-In-Aid (13BGIA17150004) from the American Heart Association. JBP was supported by a Ruth L. Kirschstein NRSA F32 NIH training grant (5F32HL123323-03).

Address correspondence to: Eric N. Olson, Department of Molecular Biology, 5323 Harry Hines Boulevard, Dallas, Texas, 75390-9148, USA. Phone 214.648.1187; Email: eric.olson@utsouthwestern.edu.

1. Mercuri E, Muntoni F. Muscular dystrophies. *Lancet*. 2013;381(9869):845–860.
2. Bertini E, D'Amico A, Gualandi F, Petrini S. Congenital muscular dystrophies: a brief review. *Semin Pediatr Neurol*. 2011;18(4):277–288.
3. Rahimov F, Kunkel LM. The cell biology of disease: cellular and molecular mechanisms underlying muscular dystrophy. *J Cell Biol*. 2013;201(4):499–510.
4. Sewry CA. Pathological defects in congenital myopathies. *J Muscle Res Cell Motil*. 2008;29(6-8):231–238.
5. Sambuughin N, et al. Dominant mutations in KBTBD13, a member of the BTB/Kelch family, cause nemaline myopathy with cores. *Am J Hum Genet*. 2010;87(6):842–847.
6. Ravenscroft G, et al. Mutations in KLHL40 are a frequent cause of severe autosomal-recessive nemaline myopathy. *Am J Hum Genet*. 2013;93(1):6–18.
7. Gupta VA, et al. Identification of KLHL41 mutations implicates BTB-Kelch-mediated ubiquitination as an alternate pathway to myofibrillar disruption in nemaline myopathy. *Am J Hum Genet*. 2013;93(6):1108–1117.
8. Garg A, et al. KLHL40 deficiency destabilizes thin filament proteins and promotes nemaline myopathy. *J Clin Invest*. 2014;124(8):3529–3539.
9. Wallgren-Pettersson C, Sewry CA, Nowak KJ, Laing NG. Nemaline myopathies. *Semin Pediatr Neurol*. 2011;18(4):230–238.
10. Dhanoa BS, Cogliati T, Satish AG, Bruford EA, Friedman JS. Update on the Kelch-like (KLHL) gene family. *Hum Genomics*. 2013;7:13.
11. Canning P, et al. Structural basis for Cul3 protein assembly with the BTB-Kelch family of E3 ubiquitin ligases. *J Biol Chem*. 2013;288(11):7803–7814.
12. Pintard L, Willems A, Peter M. Cullin-based ubiquitin ligases: Cul3-BTB complexes join the family. *EMBO J*. 2004;23(8):1681–1687.
13. Liu N, et al. Requirement of MEF2A, C, and D for skeletal muscle regeneration. *Proc Natl Acad Sci USA*. 2014;111(11):4109–4114.
14. Gupta VA, Beggs AH. Kelch proteins: emerging roles in skeletal muscle development and diseases. *Skelet Muscle*. 2014;4:11.
15. Lim LE, Campbell KP. The sarcoglycan complex in limb-girdle muscular dystrophy. *Curr Opin Neurol*. 1998;11(5):443–452.
16. Guiraud S, Aartsma-Rus A, Vieira NM, Davies KE, van Ommen GJ, Kunkel LM. The pathogenesis and therapy of muscular dystrophies. *Annu Rev Genomics Hum Genet*. 2015;16:281–308.
17. Yu W, et al. A novel human BTB-kelch protein KLHL31, strongly expressed in muscle and heart, inhibits transcriptional activities of TRE and SRE. *Mol Cells*. 2008;26(5):443–453.
18. Hwang J, Pallas DC. STRIPAK complexes: structure, biological function, and involvement in human diseases. *Int J Biochem Cell Biol*. 2014;47:118–148.
19. Guzzo RM, Sevinc S, Salih M, Tuana BS. A novel isoform of sarcolemmal membrane-associated protein (SLMAP) is a component of the microtubule organizing centre. *J Cell Sci*. 2004;117(Pt 11):2271–2281.
20. Guzzo RM, Wigle J, Salih M, Moore ED, Tuana BS. Regulated expression and temporal induction of the tail-anchored sarcolemmal-membrane-associated protein is critical for myoblast fusion. *Biochem J*. 2004;381(Pt 3):599–608.
21. Guzzo RM, Salih M, Moore ED, Tuana BS. Molecular properties of cardiac tail-anchored membrane protein SLMAP are consistent with structural role in arrangement of excitation-contraction coupling apparatus. *Am J Physiol Heart Circ Physiol*. 2005;288(4):H1810–H1819.
22. Ishikawa T, et al. A novel disease gene for Brugada syndrome: sarcolemmal membrane-associated protein gene mutations impair intracellular trafficking of hNav1.5. *Circ Arrhythm Electrophysiol*. 2012;5(6):1098–1107.
23. Nader M, et al. Tail-anchored membrane protein SLMAP is a novel regulator of cardiac function at the sarcoplasmic reticulum. *Am J Physiol Heart Circ Physiol*. 2012;302(5):H1138–H1145.
24. Arndt V, et al. Chaperone-assisted selective autophagy is essential for muscle maintenance. *Curr Biol*. 2010;20(2):143–148.
25. Kontro H, Hulmi JJ, Rahkila P, Kainulainen H. Cellular and tissue expression of DAPIT, a phylogenetically conserved peptide. *Eur J Histochem*. 2012;56(2):e18.
26. Ohsakaya S, Fujikawa M, Hisabori T, Yoshida M. Knockdown of DAPIT (diabetes-associated protein in insulin-sensitive tissue) results in loss of ATP synthase in mitochondria. *J Biol Chem*. 2011;286(23):20292–20296.
27. Päivärinne H, Kainulainen H. DAPIT, a novel protein down-regulated in insulin-sensitive tissues in streptozotocin-induced diabetes. *Acta Diabetol*. 2001;38(2):83–86.
28. Kontro H, Cannino G, Rustin P, Dufour E, Kainulainen H. DAPIT over-expression modulates glucose metabolism and cell behaviour in HEK293T cells. *PLoS ONE*. 2015;10(7):e0131990.
29. Fröhlich T, et al. Progressive muscle proteome changes in a clinically relevant pig model of Duchenne muscular dystrophy. *Sci Rep*. 2016;6:33362.
30. Sandoz PA, van der Goot FG. How many lives does CLIMP-63 have? *Biochem Soc Trans*. 2015;43(2):222–228.
31. Klopfenstein DR, Kappeler F, Hauri HP. A novel direct interaction of endoplasmic reticulum with microtubules. *EMBO J*. 1998;17(21):6168–6177.
32. Shibata Y, Shemesh T, Prinz WA, Palazzo AF, Kozlov MM, Rapoport TA. Mechanisms determining the morphology of the peripheral ER. *Cell*. 2010;143(5):774–788.
33. Fürst DO, Goldfarb LG, Kley RA, Vorgerd M, Olivé M, van der Ven PF. Filamin C-related myopathies: pathology and mechanisms. *Acta Neuropathol*. 2013;125(1):33–46.
34. Chevessier F, et al. Myofibrillar instability exacerbated by acute exercise in filaminopathy. *Hum Mol Genet*. 2015;24(25):7207–7220.
35. Abou-Elhamd A, et al. Klhl31 attenuates β-catenin dependent Wnt signaling and regulates embryo myogenesis. *Dev Biol*. 2015;402(1):61–71.
36. Thompson TG, et al. Filamin 2 (FLN2): A muscle-specific sarcoglycan interacting protein. *J Cell Biol*. 2000;148(1):115–126.
37. Faulkner G, et al. FATZ, a filamin-, actinin-, and telethonin-binding protein of the Z-disc of skeletal muscle. *J Biol Chem*. 2000;275(52):41234–41242.
38. Frey N, Olson EN. Calsarcin-3, a novel skeletal muscle-specific member of the calsarcin family, interacts with multiple Z-disc proteins. *J Biol Chem*. 2002;277(16):13998–14004.
39. Takada F, et al. Myozenin: an alpha-actinin- and gamma-filamin-binding protein of skeletal muscle Z lines. *Proc Natl Acad Sci U S A*. 2001;98(4):1595–1600.
40. van der Ven PF, et al. Indications for a novel muscular dystrophy pathway. gamma-filamin, the muscle-specific filamin isoform, interacts with myotilin. *J Cell Biol*. 2000;151(2):235–248.
41. Kley RA, et al. Pathophysiology of protein aggregation and extended phenotyping in filaminopathy. *Brain*. 2012;135(Pt 9):2642–2660.
42. Spaich S, et al. F-box and leucine-rich repeat protein 22 is a cardiac-enriched F-box protein that regulates sarcomeric protein turnover and is essential for maintenance of contractile function in vivo. *Circ Res*. 2012;111(12):1504–1516.
43. Frank D, Frey N. Cardiac Z-disc signaling network. *J Biol Chem*. 2011;286(12):9897–9904.
44. Olivé M, Kley RA, Goldfarb LG. Myofibrillar myopathies: new developments. *Curr Opin Neurol*. 2013;26(5):527–535.
45. Sarparanta J, et al. Mutations affecting the cytoplasmic functions of the co-chaperone DNAJB6 cause limb-girdle muscular dystrophy. *Nat Genet*. 2012;44(4):450–455.
46. Bonne G, et al. Mutations in the gene encoding lamin A/C cause autosomal dominant Emery-Dreifuss muscular dystrophy. *Nat Genet*. 1999;21(3):285–288.
47. Hara Y, et al. A dystroglycan mutation associated with limb-girdle muscular dystrophy. *N Engl J Med*. 2011;364(10):939–946.
48. Duggan DJ, Gorospe JR, Fanin M, Hoffman EP, Angelini C. Mutations in the sarcoglycan genes in patients with myopathy. *N Engl J Med*. 1997;336(9):618–624.
49. Cadot B, Gache V, Gomes ER. Moving and positioning the nucleus in skeletal muscle - one step at a time. *Nucleus*. 2015;6(5):373–381.
50. Metzger T, et al. MAP and kinesin-dependent nuclear positioning is required for skeletal muscle function. *Nature*. 2012;484(7392):120–124.
51. Gundersen GG, Worman HJ. Nuclear positioning. *Cell*. 2013;152(6):1376–1389.
52. Kudryashova E, Kudryashov D, Kramerova I, Spencer MJ. Trim32 is a ubiquitin ligase mutated in limb girdle muscular dystrophy type 2H that binds to skeletal muscle myosin and ubiquitinates actin. *J Mol Biol*. 2005;354(2):413–424.
53. Schoser BG, Frosk P, Engel AG, Klutzny U, Lochmüller H, Wrogemann K. Commonality of TRIM32 mutation in causing sarcotubular myopathy and LGMD2H. *Ann Neurol*. 2005;57(4):591–595.
54. LaBeau-DiMenna EM, Clark KA, Bauman KD, Parker DS, Cripps RM, Geisbrecht ER. Thin, a Trim32 ortholog, is essential for myofibril stability and is required for the integrity of the costamere in Drosophila. *Proc Natl Acad Sci U S A*. 2012;109(44):17983–17988.
55. Selcen D, Engel AG. In: Pagon RA, et al, eds. *GeneReviews(R)*. Seattle (WA): University of Washington, Seattle; 1993–2017.
56. Claeys KG, Fardeau M. Myofibrillar myopathies. *Handb Clin Neurol*. 2013;113:1337–1342.

57. Long C, McAnally JR, Shelton JM, Mireault AA, Bassel-Duby R, Olson EN. Prevention of muscular dystrophy in mice by CRISPR/Cas9-mediated editing of germline DNA. *Science*. 2014;345(6201):1184–1188.
58. Cong L, et al. Multiplex genome engineering using CRISPR/Cas systems. *Science*. 2013;339(6121):819–823.
59. Millay DP, et al. Genetic manipulation of dysferlin expression in skeletal muscle: novel insights into muscular dystrophy. *Am J Pathol*. 2009;175(5):1817–1823.
60. Naya FJ, Mercer B, Shelton J, Richardson JA, Williams RS, Olson EN. Stimulation of slow skeletal muscle fiber gene expression by calcineurin in vivo. *J Biol Chem*. 2000;275(7):4545–4548.
61. Anderson DM, et al. Severe muscle wasting and denervation in mice lacking the RNA-binding protein ZFP106. *Proc Natl Acad Sci U S A*. 2016;113(31):E4494–E4503.
62. Lim KL, et al. Parkin mediates nonclassical, proteasomal-independent ubiquitination of synphilin-1: implications for Lewy body formation. *J Neurosci*. 2005;25(8):2002–2009.